Simulations of Coalescing Neutron Star and Black Hole Binaries

Maximilian RUFFERT[1,*] and H.-Thomas JANKA[2,**]

[1] *Department of Mathematics and Statistics, University of Edinburgh Scotland EH9 3JZ, U.K.*

[2] *Max-Planck-Institut für Astrophysik, Postfach 1523, 85740 Garching, Germany*

(Received August 28, 1999)

We investigate the dynamics and evolution of merging neutron stars, of neutron stars coalescing with stellar-mass black holes, and the formation and properties of accretion tori around the (remnant) black holes.

The three-dimensional Newtonian hydrodynamics equations are integrated by a Eulerian PPM code on four nested Cartesian grids. The code includes the emission and backreaction of gravitational waves as well as a physical nuclear equation-of-state [Lattimer & Swesty 1991] and the neutrino emission from the hot matter. Lepton number and energy losses of the gas due to neutrino emission are treated by an elaborate neutrino leakage scheme which takes into account neutrinos and antineutrinos of all flavors. Neutrino-antineutrino annihilation in the vicinity of the merger is evaluated in a post-processing step. The gravity of the black hole is described with a Newtonian or, alternatively, with a Paczyński-Wiita potential. The hydrodynamic effect of the black hole is simulated by extracting all matter that flows into a sphere with radius equal to the Schwarzschild radius of the black hole or, in accretion simulations, twice the Schwarzschild radius.

The NS/NS and BH/NS merging models yield information about gravitational wave and neutrino emission. Also, they allow us to determine the physical properties (masses, densities, temperatures, estimated life times) of the remnants of the mergers: a black hole surrounded by an accretion torus. In the NS/NS case, a thick disk with a mass around $0.1\,M_\odot$ forms after the massive and very compact central object that contains most of the mass of the merged neutron stars, has collapsed to a black hole, presumably on a dynamical time scale. The dynamics of BH/NS mergers is very sensitive to the neutron star to black hole mass ratio. For low ratios the neutron star transfers mass to the black hole during a few cycles of orbital decay and subsequent widening before finally being disrupted, whereas for ratios near unity the neutron star is already destroyed during its first approach. A gas mass of about $0.5\,M_\odot$ is left in an accretion torus around the black hole.

The accretion tori radiate neutrinos at luminosities of up to several 10^{53} erg/s. Higher luminosities are found for larger disk masses and smaller black holes. The emitted neutrinos and antineutrinos annihilate into $e^\pm$ pairs with efficiencies of a few percent and rates of up to $\sim 2 \times 10^{52}$ erg/s, releasing an estimated energy of up to $\sim 10^{51}$ erg in a pair-plasma fireball. The torus geometry favors relativistic expansion of the pair plasma along the baryon depleted system axis. The occurrence of moderately beamed jets with opening angles of several ten degrees is therefore likely. The jet energies and short accretion times of the tori of about 0.1 s are in the right range to account for the subclass of short and less energetic gamma-ray bursts.

§1. Some observational quantities of gamma-ray bursts

On average, gamma-ray bursts are observed at a rate of one per day by the Burst and Transient Source Experiment (BATSE) on the Compton Gamma Ray Observatory (CGRO) [Meegan et al. (1999)]. Current theoretical estimates of the merging

*) E-mail address: m.ruffert@ed.ac.uk

**) E-mail address: thj@mpa-garching.mpg.de

rates of neutron stars and black holes are as high as 500 per day in the universe and could be 5 times more frequent than NS/NS mergers [for recent numbers, see Fryer, Woosley & Hartmann (1999); Bethe & Brown (1998) and (1999)]. Redshift measurements of half a dozen GRBs of around $z = 1 - 3$ [e.g., Metzger et al. (1997); Kulkarni et al. (1998); Djorgovski et al. (1998)] not only confirm their cosmologic nature (also suggested by their isotropic distribution over the sky) but also allow one to extrapolate the observed fluences on Earth to the total energy released in photons by the source assuming isotropic emission: gamma-ray energies up to $10^{52} - 10^{54}$ erg could be involved.

On the other hand, the duration of the bursts is fairly short and the distribution bimodal: roughly 1/3 of the bursts are 0.1–1 s long, while the majority are $10 - 100$ s [Kouveliotou et al. (1993); Mukherjee et al. (1998)]. The light curve of each GRB is very variable and in particular for long bursts very complex with fluctuation time scales down to ms, and also the curves are very different from burst to burst [e.g., Fishman & Meegan (1995)]. These short timescales and high variability indicate that compact objects must be involved in the central engine of GRBs [Paczyński (1986); Fenimore & Ramirez-Ruiz (1999)].

The spectra of GRBs are non-thermal with maxima between 100 keV and a few MeV [Klebesadel et al. (1973); Band et al. (1993)]. The generation of these photons and of the afterglow (observed at lower energies all the way down to radio waves) seems to be explained by the internal-external shock fireball model [Rees & Mészáros (1992); Sari & Piran (1997)]. This scenario is fairly independent of the exact nature of the central engine and only requires an initial variable, highly relativistic, baryon poor outflow [Mészáros & Rees (1993)].

Merging neutron stars and black holes are strong sources of gravitational waves to be measured with the upcoming large interferometers (LIGO, VIRGO, GEO600, TAMA) and are considered as promising candidates for the origin of gamma-ray bursts (GRBs) [e.g., Blinnikov et al. (1984); Eichler et al. (1989); Paczyński (1991); Narayan, Piran & Shemi (1992); Mészáros (1999)], at least for the subclass of less complex and less energetic short and hard bursts [Mao, Narayan & Piran (1994)] with typical durations of fractions of a second [Popham, Woosley & Fryer (1999); Ruffert & Janka (1999)]. Optical counterparts and afterglows of these short bursts have not yet been observed.

The fireball model is not part of our investigation. We concentrate on whether the NS-NS and NS-BH coalescence scenario is a viable explanation for the GRB central engine to meet the huge energy requirements on the short timescales observed.

§2. Computational procedures and initial conditions

Here we will only summarise the computational procedures that we used. Details of the hydrodynamic method as well as the neutrino relevant algorithms can be found in [Ruffert et al. (1997)]. The nested grid is described in [Ruffert & Janka (1998) and Ruffert (1992)]. The implementation of the black hole is explained in [Ruffert & Janka (1999)] and also in [Eberl (1998)].

The hydrodynamical simulations were done with a code based on the Piecewise

Parabolic Method (PPM) developed by Colella & Woodward (1984). The code is basically Newtonian, but contains the terms necessary to describe gravitational-wave emission and the corresponding back-reaction on the hydrodynamical flow [Blanchet et al. (1990)]. The modifications that follow from the gravitational potential are implemented as source terms in the PPM algorithm. The necessary spatial derivatives are evaluated as standard centered differences on the grid.

In order to describe the thermodynamics of the neutron star matter, we use the equation of state (EOS) of [Lattimer & Swesty (1991)] for a compressibility modulus of bulk nuclear matter of $K = 180\,\mathrm{MeV}$ in tabular form. Energy loss and changes of the electron abundance due to the emission of neutrinos and antineutrinos are taken into account by an elaborate "neutrino leakage scheme". The energy source terms contain the production of all types of neutrino pairs by thermal processes and additionally of electron neutrinos and antineutrinos by lepton captures onto baryons. The latter reactions act as sources or sinks of lepton number, too, and are included as source terms in a continuity equation for the electron lepton number. Matter is rendered optically thick to neutrinos due to the main opacity producing reactions which are neutrino-nucleon scattering and absorption of electron-type neutrinos onto nucleons.

The presented simulations were done on multiply nested and refined grids. With an only modest increase in CPU time, the nested grids allow one to simulate a substantially larger computational volume while at the same time they permit a higher local spatial resolution of the merging stars. The former is important to follow the fate of matter that is flung out to distances far away from the collision site either to become unbound or to eventually fall back. The latter is necessary to adequately resolve the strong shock fronts and steep discontinuities of the plasma flow that develop during the collision. The procedures used here are based on the algorithms that can be found in [Berger & Colella (1989), Berger (1987) and Berger & Oliger (1984)]. Each grid had 64^3 zones, the size of the smallest zone was $\Delta x = \Delta y = \Delta z = 0.64$ or $0.78\,\mathrm{km}$ in case of binary NSs and 1.25 or $1.5\,\mathrm{km}$ for BH/NS mergers. The zone sizes of the next coarser grid levels were doubled to cover a volume of 328 or $400\,\mathrm{km}$ side length for NS/NS and 640 or $768\,\mathrm{km}$ for BH/NS simulations.

In a post-processing step, performed after the hydrodynamical evolution had been calculated, we evaluated our models for neutrino-antineutrino ($\nu\bar{\nu}$) annihilation in the surroundings of the collided stars in order to construct a map showing the local energy deposition rates per unit volume. Spatial integration finally yields the total rate of energy deposition outside the neutrino emitting high-density regions.

Table I gives a list of computed NS/NS and BH/NS merger models. Besides the baryonic mass of the neutron star and the mass of the black hole, the spins of the neutron stars were varied. "Solid" means synchronously rotating stars, "none" irrotational cases and "anti" counter-rotation, i.e., spin angular momenta opposite to the direction of the orbital angular momentum vector [cf. Bildsten & Cutler (1992)]. The cool neutron stars have a radius of about $15\,\mathrm{km}$ [Ruffert, Janka & Schäfer (1996)] and the runs were started with a center-to-center distance of $42 - 46\,\mathrm{km}$ for NS/NS and with $47\,\mathrm{km}$ in case of BH/NS for $M_{\mathrm{BH}} = 2.5\,M_\odot$, $57\,\mathrm{km}$ for $M_{\mathrm{BH}} = 5\,M_\odot$ and $72\,\mathrm{km}$ for $M_{\mathrm{BH}} = 10\,M_\odot$. The simulations were stopped at a time t_{sim} between

Table I. NS/NS and BH/NS merger simulations.

Model	Type	Masses $M_\odot$	Spin	$t_{\rm sim}$ ms	$t_{\rm ns}$ ms	$d_{\rm ns}$ km	$M_{\rm ns}^{\rm min}$ $M_\odot$	$\Delta M_{\rm ej}$ $M_\odot/100$
S64	NS/NS	1.2+1.2	solid	10	2.8	15	...	2.0
D64	NS/NS	1.2+1.8	solid	13	7.3	15	...	3.8
V64	NS/NS	1.6+1.6	anti	10	3.7	15	...	0.0085
A64	NS/NS	1.6+1.6	none	10	1.7	15	...	0.23
B64	NS/NS	1.6+1.6	solid	10	1.6	15	...	2.4
TN10	BH/AD	2.9+0.26	solid	15	...	...	...	...
C2.5	BH/NS	2.5+1.6	anti	10	2.6	11	0.78	0.01
A2.5	BH/NS	2.5+1.6	none	10	4.3	18	0.78	0.03
B2.5	BH/NS	2.5+1.6	solid	10	6.0	23	0.78	0.2
C5	BH/NS	5.0+1.6	anti	15	9.1	76	0.40	2.5
A5	BH/NS	5.0+1.6	none	20	16.3	65	0.52	2.5
B5	BH/NS	5.0+1.6	solid	15	10.8	79	0.50	5.6
C10	BH/NS	10.0+1.6	anti	10	8.0	96	0.65	2.2
A10	BH/NS	10.0+1.6	none	10	9.3	95	0.60	3.2
B10	BH/NS	10.0+1.6	solid	10	5.1	97	0.65	10.0

10 ms and 20 ms. The black hole was treated as a point mass at the center of a sphere with radius $R_{\rm s} = 2GM_{\rm BH}/c^2$ which gas could enter unhindered. Its mass and momentum were updated along with the accretion of matter. Model TN10, which is added for comparison, is a continuation of the NS/NS merger model B64 where at time $t_{\rm sim} = 10$ ms the formation of a black hole was assumed and the accretion was followed for another 5 ms until a steady state was reached [Ruffert & Janka (1999)].

§3. Results

The results of our models can only be outlined in this paper. The results pertaining to the accretion of a high-density torus by a black hole can be found in [Ruffert & Janka (1999)]. The neutron star merging simulations will be published fully in [Ruffert & Janka (2000)], while the neuton star – black hole simulations are shown in detail in [Eberl (1998)] and [Janka et al. (1999)].

3.1. *Coalescing neutron star binaries*

We started our simulations with two identical Newtonian neutron stars, each having a baryonic mass of about 1.63 $M_\odot$ and a radius of 15 km, which were placed at a center-to-center distance of 42 km. The distributions of density ρ and electron fraction $Y_e \equiv n_e/n_b$ (with n_e being the number density of electrons minus that of positrons, and n_b the baryon number density) were taken from a one-dimensional model of a cold, deleptonized neutron star in hydrostatic equilibrium and were the same as in [Ruffert et al. (1996)]. For numerical reasons the surroundings of the neutron stars cannot be treated as completely evacuated. The density of the ambient medium was set to less than 10^8 g/cm^3, more than six orders of magnitude smaller than the central densities of the stars. The total mass on the whole grid, associated

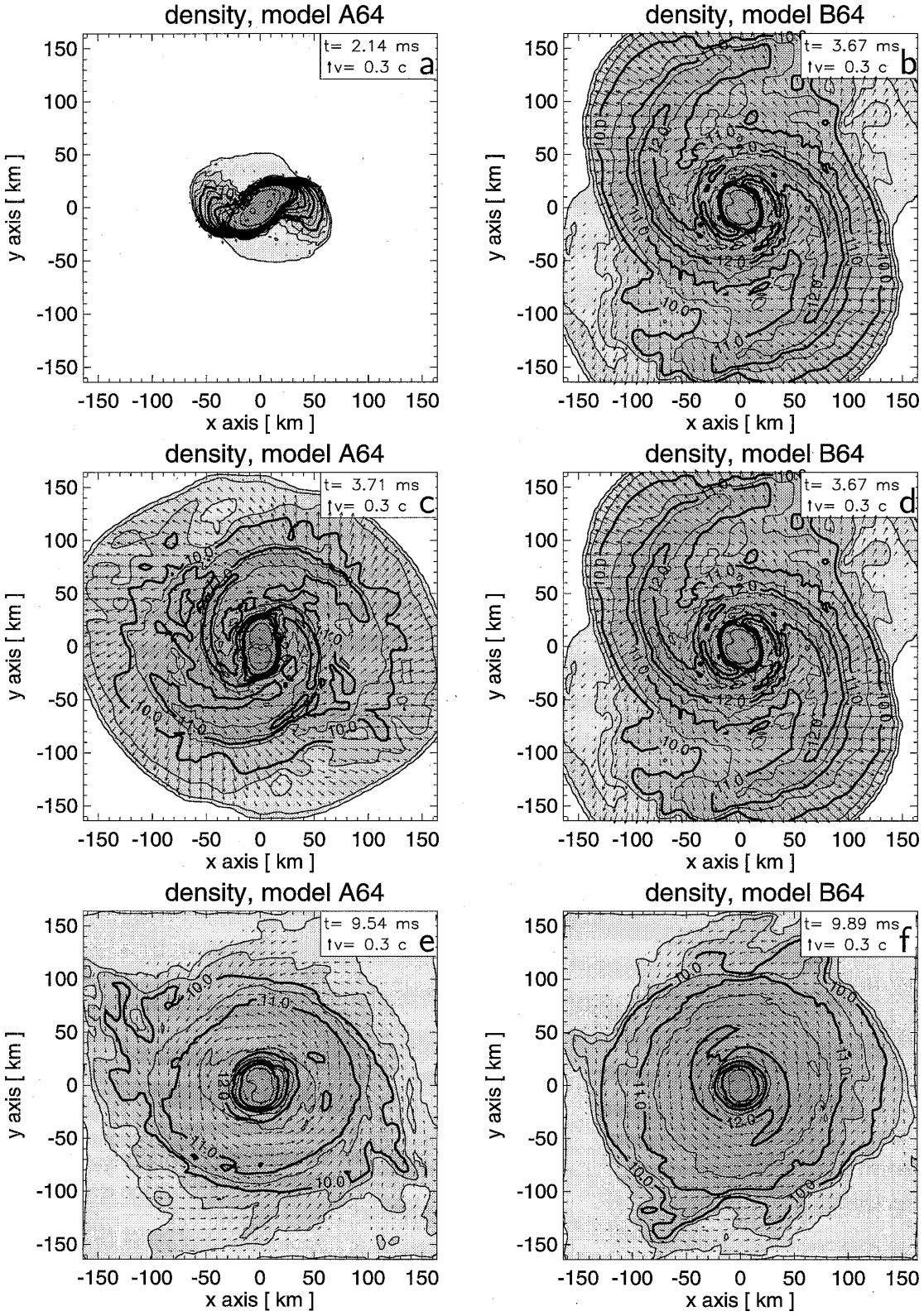

Fig. 1. Contour plots of Model A64 (left panels) and B64 (right panels) showing cuts in the orbital plane. The density is displayed together with the velocity field. The density is measured in g cm^{-3} and its contours are spaced logarithmically with intervals of 0.5 dex. The bold contours are labeled with their corresponding values. In the box in the upper right corner of each panel, a unit velocity vector and the time elapsed since the beginning of the simulation are given.

with this finite density is less than $10^{-3}\,M_\odot$.

We prescribed the orbital velocities of the coalescing neutron stars according to the motions of point masses, as computed from the quadrupole formula. The tangential components of the velocities of the neutron star centers correspond to Kepler velocities on circular orbits, while the radial velocity components reflect the emission of gravitational waves leading to the inspiral of the orbiting bodies.

A spin of the neutron stars around their respective centers was added and varied from model to model: Model A64 does not have any additional spins added on top of its orbital velocity. In this case all parts of the neutron stars start out with the same absolute value of the velocity, also called 'irrotational' motion. The angular velocity (both magnitude and direction) of the spin in Model B64 is equal to the angular velocity of the orbit. This results in a 'solid body' type motion also called 'corotating'. Model V64 is a counter-rotating case where spins and orbital angular momentum vectors have opposite directions.

Figure 1 shows the temporal evolution of the density distribution in the orbital plane for both Models A64 and B64. Initially, the orbits of the two neutron stars decay due to gravitational radiation and the stars approach each other slowly. Once the distance decreases below the instability limit the final plunge occurs (panels a & b). Note that Model B64, which has more total angular momentum, develops prominent spiral arms (panel d) in which matter is flung out to large distances. Model A64, on the contrary, remains more compact during this dynamical merging phase (panel c). However, after 10 ms when a quasi-steady state has been reached, the densities in the thick tori surrounding the merged objects are fairly similar (panels e & f).

3.2. *Black hole – thick disk accretion*

We assume that the compact object that formed during the merging of two neutron stars collapses to a black hole on a dynamical time scale of a few milliseconds after the merger. For the simulations of the formation of the accretion torus which we describe here, the merger model B64 (cf. previous section) was used as initial condition.

Two sequences of models were done, starting at different post-merging times, one in which the black-hole potential was represented by a Newtonian potential (model TN10),

$$\Phi_{\mathrm{N}} = -\frac{GM_{\mathrm{BH}}}{r} \tag{3·1}$$

and a second sequence of models (Model TP10) in which the gravitational potential was described by the Paczyński-Wiita expression,

$$\Phi_{\mathrm{PW}} \equiv -\frac{GM_{\mathrm{BH}}}{r - R_{\mathrm{s}}} \tag{3·2}$$

[Paczyński & Wiita (1980)]. This allows one to reproduce the existence and the effects of a last stable circular orbit at a radius of $3R_{\mathrm{s}} = 6GM_{\mathrm{BH}}/c^2$. We hope that this approximation, although crude, can give us some indication of the sensitivity of our results to the inclusion of proper general relativity in the modeling.

In these accretion models the inner vacuum sphere that represents the black

hole at the center of the computational grid was set to a radius of $2R_s$ instead of $1R_s$ as in the BH/NS merger simulations. The loss of mass, momentum, angular momentum and energy from the gas outside the black hole boundary were also monitored during the simulations. In the grid zones that are located inside the vacuum sphere (these zones were not removed from the hydrodynamic grid), the mass density was continuously reset to a negligibly small but finite value of 10^8 g cm^{-3} and a correspondingly very small value of the pressure was present.

The density structure of the accretion torus in the quasi-stationary state is shown in Fig. 2 for the Newtonian Model TN10 (left panels) and for the Paczyński-Wiita

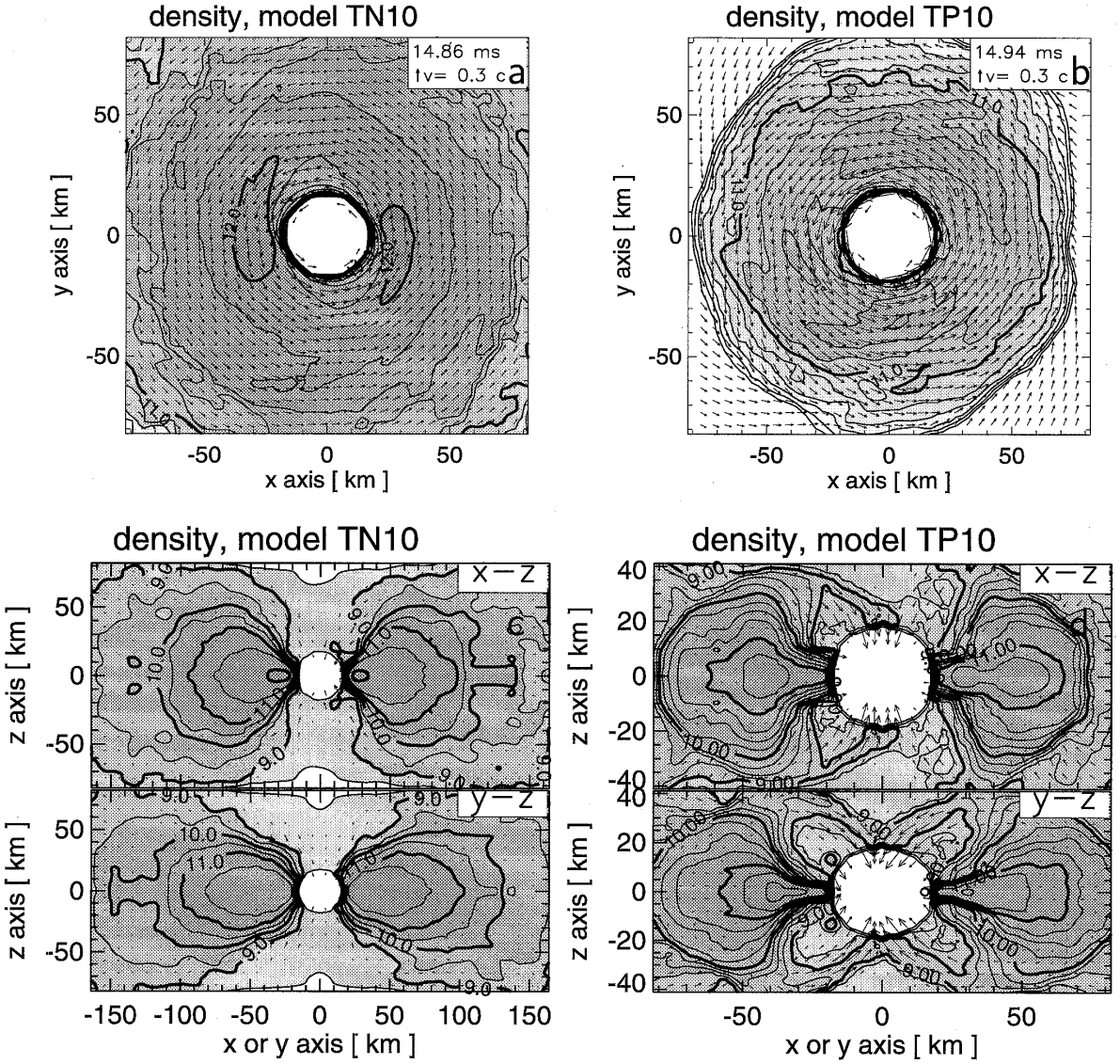

Fig. 2. Contour plots of the Newtonian Model TN10 (left panels) and Paczyński-Wiita Model TP10 (right panels) in the equatorial plane (upper figures) and perpendicular to it (lower figures) near the end of the simulation. The density is displayed together with the velocity field. The density is measured in g cm^{-3} and its contours are spaced logarithmically with intervals of 0.5 dex. The bold contours are labeled with their corresponding values. In the box in the upper right corner of the upper figures, a unit velocity vector and the time elapsed since the beginning of the simulation are given.

Model TP10 (right panels) at the end of the simulations. Contour plots in the equatorial plane are shown in panels a & b while below the situation in the x-z- and y-z-planes perpendicular to the equatorial plane is shown. At the end of the simulations the tori have become nearly axially symmetric with only minor deviations. Two higher-density hot knots are present near the inner grid boundary at $2R_\mathrm{s}$. They continue to carry the memory of the two very prominent spiral arms which were formed during the neutron star merging, grew right afterwards, and were wound up into the toroid around the black hole during the subsequent evolution. The torus of Model TP10 is smaller than the torus of Model TN10. In the former the $\rho = 10^{10}\,\mathrm{g\,cm^{-3}}$ contour is at $70 - 80\,\mathrm{km}$ whereas it extends out to $120 - 130\,\mathrm{km}$ in the latter. There are two reasons for that. On the one hand, the gas mass which remains around the black hole is smaller and on the other hand the gravitational potential is stronger in the Paczyński-Wiita case. Despite of a difference of a factor 7 in the torus mass, both models have average densities which differ only by a factor 3 (about $3 \times 10^{11}\,\mathrm{g\,cm^{-3}}$ for Model TN10 compared to approximately $10^{11}\,\mathrm{g\,cm^{-3}}$ in case of Model TP10).

The perpendicular cuts (Fig. 2, lower panels) confirm the nearly axially symmetric structure of the tori in Models TN10 and TP10 at the end of the simulations. Again, some differences between the x-z- and y-z-cuts reflect the last remainders of the spiral arms which have been inflated and dissolved into the tori. Near the poles of the black hole and along the system axis, the density has decreased to values below $5 \times 10^8\,\mathrm{g\,cm^{-3}}$. This is only one order of magnitude above the lower density limit which was set to $5 \times 10^7\,\mathrm{g\,cm^{-3}}$ in the surroundings of the torus for numerical reasons, but nevertheless it is more than $3 - 4$ orders of magnitude below the average densities inside the tori. In this sense we see the formation of an "evacuated", cylindrical funnel along the rotational axis of the black hole – torus system. Material which was swept into the polar regions during and immediately after the merging of the neutron stars falls into the newly formed black hole very quickly within a free-fall time scale because it is not supported by centrifugal forces. A comparison of the initial condition for the torus simulations of Models TN10 and TP10 (corresponding to the situation at $t \approx 10\,\mathrm{ms}$ in Model B64, cf. previous section) with the quasi-stationary states about 5 ms later reveals this rapid cleaning of the axial funnel.

3.3. *Neutron star – black hole mergers*

Due to the emission of gravitational waves the orbital separation decreases. The evolution of the density distributions of the BH/NS merger Models A5 and B5 is shown in Fig. 3. During its first approach, the neutron star transfers matter to the black hole at huge rates of several 100 up to $\sim 1000\,M_\odot/\mathrm{s}$ (Fig. 3, panels a & b). Within $2 - 3\,\mathrm{ms}$ it loses $50 - 75\%$ of its initial mass. In case of the $2.5\,M_\odot$ black hole the evolution is catastrophic and the neutron star is immediately disrupted. A mass of $0.2 - 0.3\,M_\odot$ remains in a thick disk around the black hole (M_d in Table III). In contrast, the orbital distance increases again for $M_\mathrm{BH} = 5\,M_\odot$ and $M_\mathrm{BH} = 10\,M_\odot$ and a significantly less massive neutron star begins a second approach (Fig. 3c). Again, the black hole swallows gas at rates of more than $100\,M_\odot/\mathrm{s}$. Even a third

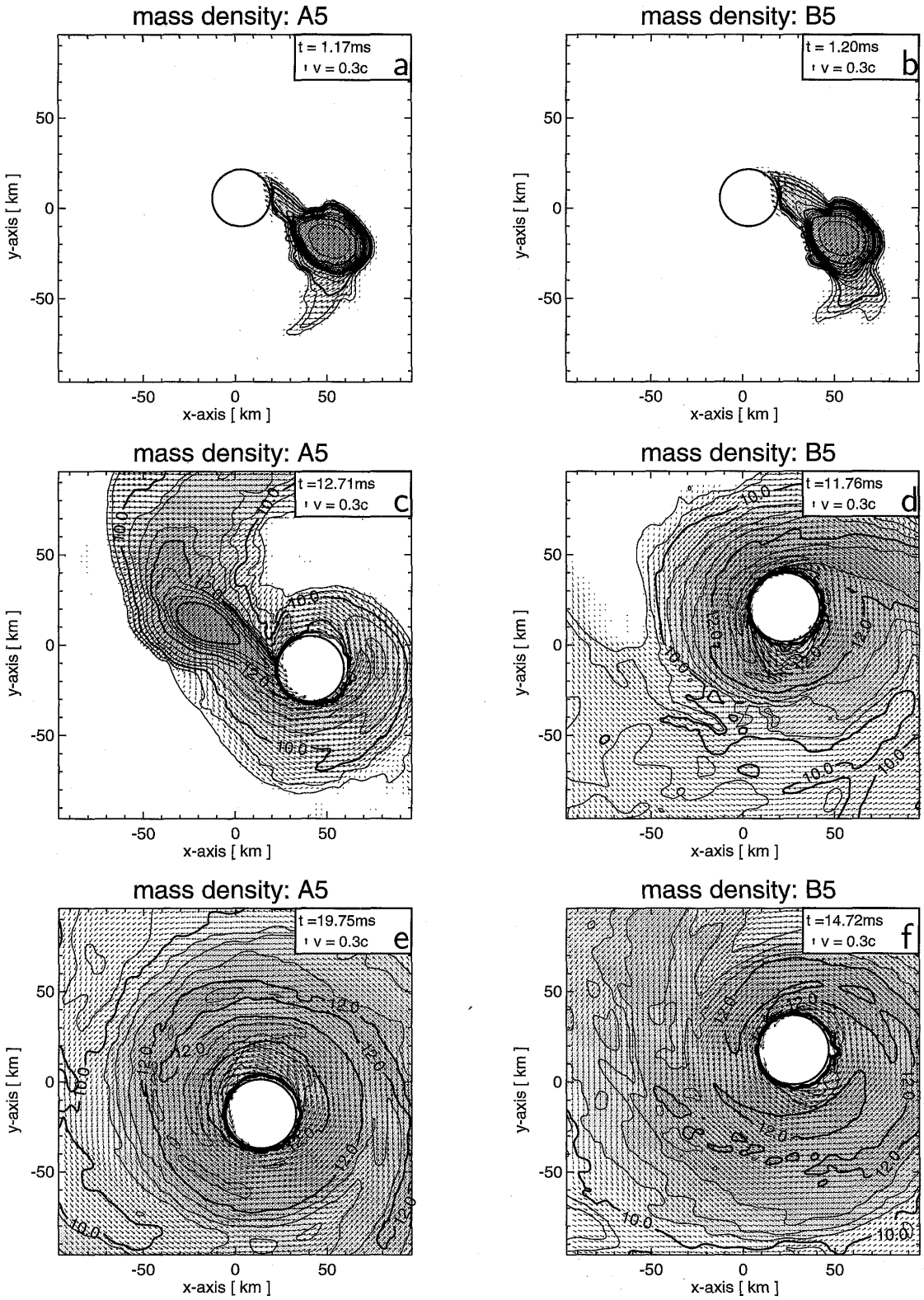

Fig. 3. Contour plots of Models A5 (left panels) and B5 (right panels) showing cuts in the orbital plane. The density is displayed together with the velocity field. The density is measured in g cm^{-3} and its contours are spaced logarithmically with intervals of 0.5 dex. The bold contours are labeled with their corresponding values. In the box in the upper right corner of each panel, a unit velocity vector and the time elapsed since the beginning of the simulation are given.

Table II. Gravity waves and neutrinos from NS/NS and BH/NS mergers.

Model	$L_{\rm GW}^{\rm max}$ $10^4\,\frac{\rm foe}{\rm s}$ [a]	$rh^{\rm max}$ 10^4cm	$E_{\rm GW}$ foe	$L_{\nu_e}^{\rm max(av)}$ $100\,\frac{\rm foe}{\rm s}$	$L_{\bar\nu_e}^{\rm max(av)}$ $100\,\frac{\rm foe}{\rm s}$	$L_{\Sigma\nu_x}^{\rm max(av)}$ $100\,\frac{\rm foe}{\rm s}$	E_ν foe	$kT^{\rm max}$ MeV	$\langle\epsilon_{\nu_e}\rangle$ MeV	$\langle\epsilon_{\bar\nu_e}\rangle$ MeV	$\langle\epsilon_{\nu_x}\rangle$ MeV
S64	0.7	5.5	14	0.3(0.2)	0.9(0.5)	0.3(0.2)	0.8	35	12	18	26
D64	0.4	5.5	13	0.5(0.3)	1.3(0.8)	0.7(0.4)	1.1	35	13	19	27
V64	1.2	6.0	23	1.1(0.5)	2.6(1.3)	0.7(0.3)	1.9	69	13	19	27
A64	2.1	8.6	52	0.9(0.5)	2.6(1.3)	1.4(0.6)	2.3	39	12	18	26
B64	2.1	8.9	37	0.6(0.4)	1.8(1.1)	0.9(0.4)	1.8	39	13	19	27
TN10	...	...	...	0.5(0.4)	1.3(0.9)	0.6(0.2)	0.8	15	9	13	21
C2.5	2.3	9.9	32	1.5(0.5)	7.3(2.5)	5.2(1.9)	4.5	74	16	22	31
A2.5	2.0	9.9	50	1.8(0.5)	6.4(2.2)	3.1(1.3)	3.6	65	15	22	31
B2.5	2.1	9.6	61	0.9(0.3)	6.5(1.7)	3.6(0.9)	2.5	61	14	21	29
C5	3.9	13.0	50	0.7(0.4)	3.8(1.6)	2.5(1.1)	4.5	46	15	20	29
A5	3.2	14.8	102	0.7(0.2)	4.4(1.5)	2.8(0.8)	4.5	51	16	24	31
B5	3.4	14.5	95	0.6(0.2)	3.7(1.1)	2.5(0.6)	2.9	44	14	21	28
C10	7.1	21.9	123	0.4(0.1)	2.5(0.4)	1.2(0.1)	0.6	51	14	19	24
A10	6.9	26.2	168	0.2(0.1)	2.5(0.5)	1.2(0.2)	0.7	50	14	20	26
B10	7.3	26.2	163	0.4(0.1)	2.5(0.8)	1.4(0.2)	1.1	52	13	18	24

[a] 1 foe = 10^{51} erg (**fifty one erg**).

Table III. Accretion phase and neutrino annihilation.

Model	$M_{\rm d}$ $M_\odot$	$\dot M_{\rm d}$ $M_\odot$/s	$t_{\rm acc}$ ms	$\alpha_{\rm eff}$ 10^{-3}	$a_{\rm i}$	$a_{\rm f}$	$a_{\rm BH}^{\infty}$	$\langle L_\nu\rangle$ $100\,\frac{\rm foe}{\rm s}$ [a]	$\dot E_{\nu\bar\nu}$ foe/s	q_ν %	$q_{\nu\bar\nu}$ %	E_ν foe	$E_{\nu\bar\nu}$ foe
S64	...	...	...	...	0.98	0.75	...	1.5	1	...	1	...	...
D64	...	...	...	...	0.87	0.69	...	2	2	...	1	...	...
V64	...	...	...	...	0.64	0.49	...	4	9	...	2	...	...
A64	...	...	...	...	0.76	0.55	...	5	9	...	2	...	...
B64	...	...	...	...	0.88	0.63	...	3	7	...	2	...	...
TN10	0.26	5	53	4	...	0.42	0.59	1.2	0.5	1.3	0.4	7	0.03
C2.5	0.26	6	43	4	0.65	0.47	0.60	7	20	6	3	30	0.9
A2.5	0.33	<14	>24	<8	0.67	0.39	0.56	7	20	>3	3	>17	>0.5
B2.5	0.45	<35	>13	<14	0.69	0.38	0.61	7	20	>1	3	>9	>0.3
C5	0.38	5	76	5	0.44	0.27	0.42	4	8	4	2	30	0.6
A5	0.49	6	82	4	0.45	0.17	0.37	4	8	4	2	33	0.7
B5	0.45	6	75	5	0.46	0.19	0.38	4	8	4	2	30	0.6
C10	0.67	<10	>67	<11	0.24	0.07	0.25	2	2	>1	1	>13	>0.1
A10	0.56	<60	>9	<82	0.25	0.07	0.22	2	2	>0.2	1	>2	>0.02
B10	0.47	3	160	5	0.25	0.11	0.23	2	2	4	1	32	0.3

[a] 1 foe = 10^{51} erg (**fifty one erg**).

cycle is possible. Finally, at a distance $d_{\rm ns}$ and time $t_{\rm ns}$ the neutron star with a mass of $M_{\rm ns}^{\rm min}$ is destroyed (Table I) and most of its mass ends up in an accretion disk (Table III, Fig. 3, panels e & f). In the case of NS/NS mergers $t_{\rm ns}$ means the time when the two density maxima of the stars are a stellar radius, i.e., $d_{\rm ns} = 15\,$km, apart. The evolution of the density distribution of Models A5 and B5 are shown in Fig. 3.

During the merging a gas mass $\Delta M_{\rm ej}$ of $\sim 10^{-4}\,M_\odot$ (in case of counter-rotation

and $M_{\rm BH} = 2.5\,M_\odot$) to $\sim 0.1\,M_\odot$ (corotation and $M_{\rm BH} = 10\,M_\odot$) is dynamically ejected (Table I). In the latter case the associated angular momentum loss is about 7%, in all other cases it is less than 5% of the total initial angular momentum of the system. Another fraction of up to 24% of the initial angular momentum is carried away by gravitational waves. In Table III the rotation parameter $a = Jc/(GM^2)$ is given for the initial state of the binary system ($a_{\rm i}$) and at the end of the simulation ($a_{\rm f}$) for the remnant of NS/NS mergers or for the black hole in BH/NS systems, respectively, provided the black hole did not have any initial spin. When the whole disk mass $M_{\rm d}$ has been swallowed by the Kerr black hole, a final value $a_{\rm BH}^{\infty}$ (Table III) will be reached in case of the accretion of a corotating, thin disk with maximum radiation efficiency.

The phase of largest mass flow rate to the black hole (between 2 and 5 ms after the start of the simulations) is connected with a maximum of the gravitational wave luminosity $L_{\rm GW}$ which reaches up to 7×10^{55} erg/s (Table II). The peak values of $L_{\rm GW}$ and the wave amplitude rh (for distance r from the source) increase with the black hole mass. The total energy $E_{\rm GW}$ radiated in gravitational waves can be as much as $0.1\,M_\odot c^2$ for $M_{\rm BH} = 10\,M_\odot$.

Compressional heating, shear due to numerical viscosity and dissipation in shocks heat the gas during accretion to maximum temperatures $kT^{\rm max}$ of several 10 MeV. Average temperatures are between 5 and 20 MeV, the higher values for the less massive and more compact black holes. At these temperatures and at densities of $10^{10} - 10^{12}\,{\rm g/cm^3}$ in the accretion flow, electrons are non-degenerate and positrons abundant. Electron neutrinos and antineutrinos are therefore copiously created via reactions $p + e^- \to n + \nu_e$ and $n + e^+ \to p + \bar{\nu}_e$ and dominate the neutrino energy loss from the accreted matter. Dense and hot neutron star matter is not completely transparent to neutrinos. By taking into account the finite diffusion time, the neutrino trapping scheme limits the loss of energy and lepton number.

Maximum and average luminosities ($L_{\nu_i}^{\rm max}$ and $L_{\nu_i}^{\rm av}$, respectively) for ν_e and $\bar{\nu}_e$ and for the sum of all heavy-lepton neutrinos (which are denoted by $\nu_x \equiv \nu_\mu, \bar{\nu}_\mu, \nu_\tau, \bar{\nu}_\tau$, and which are mainly produced by e^+e^- annihilation) are given in Table II for the simulated time intervals. The total neutrino luminosities $L_\nu(t)$ fluctuate strongly with the varying mass transfer rate to the black hole during the cycles of orbital decay and widening. The total energy E_ν radiated in neutrinos in 10 – 20 ms is typically several 10^{51} erg. Time averages of the mean energies $\langle\epsilon\rangle$ of the emitted neutrinos are ~ 15 MeV for ν_e, 20 MeV for $\bar{\nu}_e$, and 30 MeV for ν_x. Luminosities as well as mean energies, in particular for smaller black holes, are significantly higher than in case of NS/NS mergers.

At the end of the simulations, several of the BH/NS models have reached a steady state, characterized by only a slow growth of the black hole mass with a nearly constant accretion rate. Corresponding rates $\dot{M}_{\rm d}$ are given in Table III and are several $M_\odot$/s. From these we estimate torus life times $t_{\rm acc} = M_{\rm d}/\dot{M}_{\rm d}$ of 50 – 150 ms. Values with $>$ and $<$ signs indicate cases where the evolution and emission are still strongly time-dependent at the end of the simulation. In these cases the accretion torus around the black hole has also not yet developed axial symmetry. In all other cases the effective disk viscosity parameter $\alpha_{\rm eff} \sim v_{\rm r}/v_{\rm Kepler} \sim 3\sqrt{6}R_{\rm s}/(t_{\rm acc}c)$,

evaluated at a representative disk radius of $3R_\mathrm{s} = 6GM_\mathrm{BH}/c^2$, has the same value, $4 - 5 \times 10^{-3}$. This value is associated with the numerical viscosity of the hydro code (which solves the Euler equations) and the chosen resolution. The further disk evolution is driven by the angular momentum transport mediated by viscous shear forces, which determine the accretion rate.

The physical value of the disk viscosity is unknown. The numerical viscosity of our code, however, is in the range where the viscous energy dissipation and the energy emission by neutrinos should be roughly equal, i.e., where the conversion efficiency $q_\nu = \langle L_\nu \rangle / (\dot{M}_\mathrm{d} c^2)$ of rest-mass energy to neutrinos is nearly maximal [see Ruffert et al. (1997); Ruffert & Janka (1999)]. Assuming that the average neutrino luminosity $\langle L_\nu \rangle$ at t_sim is representative for the subsequent accretion phase, we obtain for q_ν numbers between 4 and 6% and total energies $E_\nu \sim \langle L_\nu \rangle t_\mathrm{acc}$ around 3×10^{52} erg (Table III). Annihilation of neutrino pairs, $\nu\bar{\nu} \to e^+e^-$, deposits energy at rates up to $\dot{E}_{\nu\bar{\nu}} \sim 2 \times 10^{52}$ erg/s in the vicinity of the black hole (Fig. 4). This corresponds to total energies $E_{\nu\bar{\nu}} \sim \dot{E}_{\nu\bar{\nu}} t_\mathrm{acc}$ as high as $\sim 10^{51}$ erg and annihilation efficiencies $q_{\nu\bar{\nu}} = \dot{E}_{\nu\bar{\nu}} / \langle L_\nu \rangle$ of $1 - 3\%$.

§4. Conclusions

Black hole – accretion disk systems provide ideal conditions for efficient $\nu\bar{\nu}$ annihilation and the creation of relativistic outflow. A large fraction of the neutron star matter is swallowed by the black hole within milliseconds, but a thick disk with a mass of $\sim 0.5\,M_\odot$ forms and could be accreted on time scales of about 0.1 s. The region above the poles of the black hole contains definitely less than $10^{-5}\,M_\odot$ of baryonic matter and an energy deposition of $\sim 10^{51}$ erg by $\nu\bar{\nu}$ annihilation as obtained in several of our models should allow for relativistic expansion with a Lorentz factor $\Gamma = 1 + E_{\nu\bar{\nu}}/(Mc^2) \sim 100$. These estimates should not change much if the different effects of general relativity on $\nu\bar{\nu}$ annihilation are taken into account in combination [Ruffert & Janka (1999)]. The energy in the pair-plasma could therefore be sufficient to explain observable burst luminosities $L_\gamma \sim E_{\nu\bar{\nu}}/(f_\Omega t_\gamma)$ up to several $10^{53}\,\mathrm{erg\,s^{-1}}$ for burst durations $t_\gamma \approx 0.1 - 1$ s, if the γ emission is beamed in two moderately focussed jets into a fraction $f_\Omega = 2\delta\Omega/(4\pi) \approx 1/100 - 1/10$ of the sky. Further simulations of the merging and post-merging phases including general relativistic effects are very important.

Acknowledgements

MR would like to thank the organizers for a perfectly run conference, and YITP and the Yukawa Memorial Foundation for generous sponsorship through which participation at YKIS'99 was made possible. Work on this project was supported by the U.K. PPARC as Advanced Fellow for MR and by the DFG on grant "SFB 375 für Astro-Teilchenphysik" for HTJ. We thank T. Eberl for running the BH/NS merger simulations as work for his Diploma Thesis. The calculations were performed at the Rechenzentrum Garching of the Max-Planck Gesellschaft.

References

1) D. Band, J. Matteson, L. Ford et al., Astrophys. J. **413** (1993), 281.
2) M. J. Berger, SIAM J. Numer. Anal. **24** (1987), 967.
3) M. J. Berger and P. Colella, J. Comput. Phys. **82** (1989), 64.
4) M. J. Berger and J. Oliger, J. Comput. Phys. **53** (1984), 484.
5) H. A. Bethe and G. E. Brown, Astrophys. J. **517** (1999), 318; **506** (1998), 780.
6) L. Blanchet, T. Damour and G. Schäfer, Mon. Not. R. Astron. Soc. **242** (1990), 289.
7) S. I. Blinnikov, I. D. Novikov et al., Sov. Astron. Lett. **10** (1984), 177.
8) L. Bildsten and C. Cutler, Astrophys. J. **400** (1992), 175.
9) P. Colella and P. R. Woodward, J. Comput. Phys. **54** (1984), 174.
10) S. G. Djorgovski, S. R. Kulkarni, J. S. Bloom et al., Astrophys. J. **508** (1998), L17.
11) Th. Eberl, Diploma Thesis, Technical University Munich (1998).
12) D. Eichler, M. Livio, T. Piran and D. N. Schramm, Nature **340** (1998), 126.
13) E. E. Fenimore and E. Ramirez-Ruiz, astro-ph/9906125; in *PASP Conf. Proc. GRB.*
14) G. Fishman and C. Meegan, Ann. Rev. Astron. Astrophys. **33** (1995), 415.
15) R. W. Klebesadel, I. B. Strong and R. A. Olson, Astrophys. J. **182** (1973), L85.
16) C. Kouveliotou, C. A. Meegan, G. J. Fishman et al., Astrophys. J. **413** (1993), L101.
17) S. Kulkarni, S. G. Djorgovski, A. N. Ramaprakash et al., Nature **393** (1998), 35.
18) H.-Th. Janka, Th. Eberl, M. Ruffert and C. Fryer, in preparation.
19) J. M. Lattimer and F. D. Swesty, Nucl. Phys. **A535** (1991), 331.
20) S. Mao, R. Narayan and T. Piran, Astrophys. J. **420** (1994), 171.
21) P. Mészáros and M. Rees, Astrophys. J. **405** (1993), 278.
22) P. Mészáros, astro-ph/9904038; in *Proc. 19th Texas Symp., Paris, Dec. 1998.*
23) M. Metzger, S. G. Djorgovski, S. R. Kulkarni et al., Nature **387** (1997), 878.
24) S. Mukherjee, E. D. Feigelson, G. J. Babu et al., Astrophys. J. **508** (1998), 314.
25) R. Narayan, T. Piran and A. Shemi, Astrophys. J. **379** (1991), L17.
26) W. S. Paciesas, C. A. Meegan, G. N. Pendleton et al., Astrophys. J. Suppl. **122** (1999), 465.
27) B. Paczyński and P. J. Wiita, Astron. Astrophys. **88** (1980), 23.
28) B. Paczyński, Astrophys. J. **308** (1996), L43.
29) B. Paczyński, Acta Astron. **41** (1991), 257.
30) R. Popham, S. E. Woosley and C. Fryer, Astrophys. J. **518** (1999), 356.
31) M. Rees and P. Mészáros, Mon. Not. R. Astron. Soc. **258** (1992), P41.
32) M. Ruffert, Astron. Astrophys. **265** (1992), 82.
33) M. Ruffert, H.-Th. Janka and G. Schäfer, Astron. Astrophys. **311** (1996), 532.
34) M. Ruffert, H.-Th. Janka, K. Takahashi and G. Schäfer, Astron. Astrophys. **319** (1997), 122.
35) M. Ruffert and H.-Th. Janka, Astron. Astrophys. **338** (1998), 535.
36) M. Ruffert and H.-Th. Janka, Astron. Astrophys. **344** (1999), 573.
37) M. Ruffert and H.-Th. Janka, Astron. Astrophys. (2000), in press.
38) R. Sari and T. Piran, Astrophys. J. **485** (1997), 270.